Author(s): Wen, Chenyu; Zeng, Shuangshuang; Arstila, Kai; Sajavaara, Timo; Zhu, Yu; Zhang, Zhen; Zhang, Shi-Li

Title: A generalized noise study of solid-state nanopores at low frequencies

Year: 2017

Version:

Please cite the original version:

Wen, C., Zeng, S., Arstila, K., Sajavaara, T., Zhu, Y., Zhang, Z., & Zhang, S.-L. (2017). A generalized noise study of solid-state nanopores at low frequencies. ACS Sensors, 2(2), 300-307. https://doi.org/10.1021/acssensors.6b00826

Article

A generalized noise study of solid-state nanopores at low frequencies

Chenyu Wen, Shuangshuang Zeng, Kai Arstila, Timo Sajavaara, Yu Zhu, Zhen Zhang, and Shi-Li Zhang

ACS Sens., **Just Accepted Manuscript** • DOI: 10.1021/acssensors.6b00826 • Publication Date (Web): 06 Feb 2017

A generalized noise study of solid-state nanopores at low frequencies

Chenyu Wen,[1,‡] Shuangshuang Zeng,[1,‡] Kai Arstila,[2] Timo Sajavaara,[2] Yu Zhu,[3] Zhen Zhang,[1,] and Shi-Li Zhang[1]*

1. Division of Solid-State Electronics, Department of Engineering Sciences, Uppsala University, SE-751 21 Uppsala, Sweden

2. Department of Physics, University of Jyvaskylä, P.O. Box 35, FI-40014, Finland

3. IBM Thomas J. Watson Research Center, 1101 Kitchawan Rd., Yorktown Heights, NY 10598, USA

KEYWORDS: flicker noise, nanopore, electrical double layer, model, power spectrum density, low frequency range, Hooge's theory

ABSTRACT：The nanopore technology has been extensively investigated for analysis of biomolecules, and a success story in this field concerns DNA sequencing using a nanopore chip featuring an array of hundreds of biological nanopores (BioNs). Solid-state nanopores (SSNs) have been explored to attain longer lifetime and higher integration density than what BioNs can offer, but SSNs are generally considered to generate higher noise whose origin remains to be confirmed. Here, we systematically study low-frequency (including thermal and flicker) noise characteristics of SSNs measuring 7 to 200 nm in diameter drilled through a 20-nm thick SiN_x membrane by focused ion milling. Both bulk and surface ionic currents in the nanopore are found to contribute to the flicker noise, with their respective contributions

determined by salt concentration and *p*H value in electrolytes as well as bias conditions. Increasing salt concentration at constant *p*H and voltage bias leads to increase in the bulk ionic current and noise therefrom. Changing *p*H at constant salt concentration and current bias results in variation of surface charge density, and hence alteration of surface ionic current and noise. In addition, the noise from Ag/AgCl electrodes can become predominant when the pore size is large and/or the salt concentration is high. Analysis of our comprehensive experimental results leads to the establishment of a generalized nanopore noise model. The model not only gives an excellent account of the experimental observations, but can also be used for evaluation of various noise components in much smaller nanopores currently not experimentally available.

Nanometer-size pores formed in an insulating membrane have been developed as chemical and biological sensors for several decades,[1-4] primarily with the aim to detect DNA,[5] RNA,[6] proteins,[7] large chemical molecules,[8,9] and even small particles.[10] A success example is the use of biological or synthetic nanopores (BioNs), such as α-Hymolysin, immobilized onto a biological membrane to sequence DNA,[11-13] a pursuit that already began in the 1990's and has led to a portable DNA sequencing system MinION being commercialized by Oxford Nanopore Technologies.[14] However, nanopore sensors based on the BioN-membrane combination usually suffer from mechanical fragility with short lifetime and sensitivity to working environments.[11] Compatibility with the well-developed silicon process technology is also highly desired in order to achieve massively parallelized sequencing at low costs.[11,15] Solid-state nanopores (SSNs) have, therefore, been intensively explored in recent years as a competitive alternative to the biological ones for high-throughput sequencing of single DNA strands.

One of the major challenges with SSNs is its high background noise level,[11,16] which can severely distort the very weak signal carrying critical information of the detected molecules. Our recent simulation of DNA sequencing based on a simple nano-disc model[17] indicates that the noise level measured in current should be controlled to be at least 5 times smaller than 1% of the open-pore ionic current in order to discriminate the four nucleotides on a translocating DNA strand. Noise control requires identification of the origin and improved understanding of the characteristics of the various noise sources, which has motivated extensive research activities. In short, noise in SSNs has been studied with respect to the mechanism and characteristics of flicker noise,[18-23] dielectric noise,[24] and capacitive noise.[25] Noise generated by nanobubbles has also been considered a source of flicker noise in nanopores.[26] Dependence of noise on bandwidth,[27] leakage current,[28] device structure,[29] and surface conditions[30,31] has also been the subject of investigation. Moreover, low noise readout circuits have been designed.[32-34] However, the source of flicker noise still remains to be confirmed.[35] Furthermore, the analyses up to date are mostly single-issue-focused and a more generalized treatment that takes into account all sources and aspects of noise is necessary. In doing so, practical solutions to mitigating the noise of different origins can be outlined and implemented. Finding a generalized model, especially in the low-frequency (LF) range to which the desired translocation speed for, e.g., DNA sequencing, corresponds, is what the present work is aiming at.

In this work, we employ nanopores of different diameters from 7 to 200 nm etched through a 20-nm thick SiN_x membrane to systematically investigate the noise characteristics in the 0.1-1000 Hz range. We scrutinize how a range of parameters, including salt concentration, *p*H value, nanopore size, and bias current, affect the noise characteristics. Based on a conventional descriptive model of noise in the literature,[16,30] a generalized model encompassing all aspects and all parameters investigated is developed. The model results are

found to agree well with the experimental data. The model is further used to analyze and predict the significance of each and every noise component under different conditions, especially for nanopores of more constricted dimensions than experimentally achieved.

Results and Discussion

A. General properties of SiN_x nanopores

Our nanopores were fabricated by drilling through a 20-nm thick, suspended SiN_x membrane using focused ion beam milling with either helium (for pores of sub-10 nm in diameter) or gallium (for pores of 20 nm and above in diameter), see fabrication details in Methods. The measurement setup is shown in Figure S1 (Supplementary Information). The two electrolyte reservoirs on the two sides of the SiN_x membrane were filled with potassium chloride (KCl) solutions of equal concentration during the measurement. The micrograph in Figure 1a shows the transmission electron microscope (TEM) image of a representative nanopore achieved using helium ions. As seen, the pore has an irregular shape far from being circular. A linear current-voltage relationship shown in Figure 1b indicates an ohmic electrical property, for three salt solutions of different KCl concentrations from 10 mM to 1 M. By employing the well-established conductance model for nanopores,[36,37] an effective diameter of this particular pore is extracted to be 7.2 nm, which is illustrated by the green dash circle in the figure. The difference between the effective and observed pore size could arise from unknown surface effects on nanopore conductance. Thus in what follows, all the diameter values referred to are effective since they were determined by current measurement and subsequent model extraction.

A typical pattern of the noise power spectrum density (PSD) for the 7.2 nm nanopore is shown as Figure 1c. The noise PSD was converted from the time-domain current waveform recorded under 1 nA current bias in a 1 M KCl solution using fast Fourier transform. In the 0.1 Hz-1 kHz range, the current waveform was recorded for 30 s at 10 kHz sampling rate. For the 1 kHz-100 kHz range, the sampling was conducted for 1 s at 250 kHz. In order to reduce uncertainty, all the noise PSDs given in this paper represent the average of five measurements for each data point. The samples were cleaned in piranha solution with H_2SO_4:H_2O=3:1 and deionized water prior to the measurement and the data acquisition was not performed until the noise characteristics was stabilized. The PSD of a SSN can be described as:[16,30]

$$S_I = a_1 \frac{1}{f^{\beta}} + a_2 + a_3 f + a_4 f^2 \qquad (1)$$

where, f is frequency and $a_{1,2,3,4}$ are coefficients. It is composed of LF flicker noise a_1/f^{β} with β between[26,38] 1 and 2, white thermal noise a_2, dielectric noise[27,39] $a_3 f$, and capacitive noise[40] $a_4 f^2$. The white thermal noise shown as the black horizontal dash line in Figure 1c is calculated from the nanopore resistance by:

$$S_{IT} = a_2 = \frac{4kT}{R} \qquad (2)$$

where, k is Boltzmann constant, T is absolute temperature in degrees Kelvin, and R is the resistance of the nanopore. We could not clearly identify the capacitive noise component in our measurement, most likely because 100 kHz is still too low to allow its observation in our nanopore system. The drop of PSD beyond 30 kHz is caused by the low-pass filter in the amplifier. The high-frequency noise components, i.e. dielectric and capacitive, are mainly related to the capacitance of the system.[27,39,40] According to the geometry and material of our nanopore chip, the parasitic capacitance is estimated to be 30 pF. As the amplitude of the

capacitance noise will not become compatible with that of the 1/*f* noise at 1 Hz until the frequency is raised above 1 MHz. However, the noise in the LF range is strongly dependent on several key parameters, such as pore size, salt concentration, and *p*H value of the solution, that can be designed and engineered for optimal nanopore sensing. In the remainder of this work, we will focus on the noise behavior of nanopores in the LF range (<1 kHz). For this purpose, nanopores of relatively large diameters were used to help reveal more details and facilitate the investigation of various LF noise components with high fidelity since a large range of bias currents within the equipment compliance and a large span of KCl concentrations are both possible.

B. Dependence of LF noise on nanopore size and salt concentration

The noise PSDs of a 65-nm nanopore are shown in Figure 2a-c for measurements with three different KCl concentrations, 10 mM, 100 mM, and 1 M, respectively. For each concentration, the PSD was measured under various current biases from 5 to 100 nA. Since the maximum voltage bias allowed by the amplifier is 1 V, the ionic current cannot reach 100 nA for small-diameter nanopores or with the highly resistive 10 mM KCl solution. The PSD in the LF range is dominated by the 1/*f*-shape noise and the level of this component increases with increasing current. Further, increasing KCl concentration reduces the difference in PSDs corresponding to different current biases. In other words, the PSD is less dependent on ionic current in solutions of higher KCl concentration. This observation is in sharp contrast to the general understanding that the PSD of the flicker noise should have a current-square dependence as follows:[18,41]

$$S_{IF} = \frac{a_1}{f^{\beta}} = \frac{\alpha_H I^2}{N_C f^{\beta}} \quad (3)$$

where, α_H the Hooge parameter and N_c is the total number of conducting carriers. This relationship also indicates that lower noise is anticipated for higher salt concentration with larger N_c, at a given I. However, the opposite is observed experimentally as mentioned above, which can be better visualized using the root mean square (RMS) value of noise as shown below.

In order to identify the cause(s) responsible for such inconsistencies, possible noise sources in the measurement system were analyzed. We first found that the Ag/AgCl electrodes could generate current-independent 1/*f* noise, see Supporting Information Figure S1. We infer that this current-independency results from thermal noise that is further modulated to the 1/*f* shape,[42] rather than from flicker noise; this specific thermal noise component originates from the electrode-electrolyte interface and contributes to the PSD as a voltage source that induces current fluctuations in the nanopore resistance, see a detailed analysis in Supporting Information. Hence, it appears as a background floor at zero-bias current in the PSD, which is increased when the solution resistance of the nanopore is decreased by increasing KCl concentration and/or nanopore diameter. We will use "1/*f* noise" to denote any noise that results in the 1/*f*-shape in PSD, being aware of its different sources – the flicker noise from the ionic current and the 1/*f*-shape noise from the electrodes.

The dependence of flicker noise PSD on KCl concentration should follow eq. (3), i.e. increasing KCl concentration (increasing N_c) lowers noise, in contrast to the rising noise floor from the Ag/AgCl electrodes due to a lowered solution resistance. In effect, the decreasing PSD levels (of the flicker noise) at different current biases are pushed back by the rising noise floor (from the Ag/AgCl electrodes) and become less current dependent. Alternatively, it can be viewed as that the current-independent noise floor from the electrodes dominates at high KCl concentrations, while the current-dependent flicker noise from the nanopore itself governs at low KCl concentrations. Hence, the PSD curves at 5, 10, and 20 nA in Figure 2c

lie close to one another, which basically represents the noise floor from the Ag/AgCl electrodes. Their PSDs display a strong frequency-dependency with β=1.5, which differs from β=1 for the flicker noise of the nanopore.

The RMS values of noise from 3 Hz to 1 kHz versus current bias are depicted in Figure 2d for the three different KCl concentrations. Indeed, the noise level represented by RMS is found to be higher with 1 M than with 100 mM KCl at the same current 5 nA, which contradicts the prediction by eq. (3) for flicker noise. In accordance with the PSD characteristics, the noise RMS shows a stronger current dependency at lower KCl concentrations. Furthermore, the current dependence of the noise RMS is weakened by the growing white thermal noise (shown as the horizontal dash lines in Figure 2a-c) with increasing KCl concentration. Also seen in Figure 2d is a concentration-independent noise RMS at low current bias conditions, which is set by the noise floor from the Ag/AgCl electrodes.

The LF noise PSD for nanopores of different sizes all with the 1 M KCl solution is compared in Figure 3. The PSDs of the 20, 95, and 192 nm nanopores in Figure 3a-c, respectively, show the same pattern of development as that with the 65 nm nanopore in Figure 2. By plotting the noise RMS of all the nanopores in Figure 3d, the effects of ionic current and nanopore size as well as the development trends are clearly evident: the flicker noise becomes invisible and the 1/*f*-shape noise floor from the Ag/AgCl electrodes dictates for large-diameter pores. The weakened dependence of RMS on current with increasing pore size due to the dominance of the electrode noise is also clearly visualized. The white thermal noise level from the nanopore itself is continually raised when increasing pore size (i.e. decreasing pore resistance) seen in Figures 2c and 3a-c, which also contributes to the observed leveling-off of the noise RMS in Figure 3d. Overall, the total noise becomes more dominated by the flicker noise for smaller nanopores, as validated by the noise characteristics of the pore 7.2 nm in diameter shown in Supporting Figure S6a as well as its comparison with the other pores in

terms of noise RMS summarized in Supporting Figure S6b. Its noise PSD in Figure S5a shows a near current-square dependence, which illustrates that the 1/*f* noise in such small pores is almost totally determined by the flicker noise, as expected.

C. Origin of the nanopore flicker noise

The origin of nanopore noise in SSNs has been a subject of intensive studies and the frequency-dispersion of noise is well understood.[19] However, the constituents of flicker noise remain unclarified. The following discussion will build on our understanding of flicker noise in semiconductor devices that generally results from the fluctuation of charge carrier number and mobility.[41] For the ionic current in a nanopore, it is known to consist of two components: surface current representing the movement of ions confined within the boundary of the electrical double layer (EDL) at the pore-electrolyte interface and bulk current describing the convection flow with ions beyond EDL.[36,43,44] Thus, the source of flicker noise may also be related to these two components. The respective effects of surface and bulk current are analyzed by conducting the PSD measurements with solutions of different KCl concentrations at constant *p*H and voltage bias (Figure 4a) and with solutions of different *p*H values at constant KCl concentration and current bias (Figure 4b). Constant *p*H and voltage bias were necessary in order to attain an invariable surface current, while constant KCl concentration and current bias were applied so as to reach an invariable bulk current.

A relatively large pore measuring 95 nm in diameter was chosen in Figure 4a to minimize the potential influence of the surface thus warrant the predominant effect of the bulk. The noise was measured at a constant voltage bias of 0.1 V in order to generate a sufficiently large current so as to minimize the probable effect of the Ag/AgCl electrodes on the 1/*f* noise. Surface current is merely influenced by the surface charge whose density stays nearly

constant at a given *p*H value. According to the site binding model of EDL,[45] the variation of surface charge density on SiN_x is below 15% when the KCl concentration is varied from 1 M to 10 mM (see Supporting Figure S7). Hence, surface current should remain the same in solutions of different KCl concentrations. If surface current is the only source of flicker noise, the noise level would not change by varying KCl concentration. Thus, the results in Figure 4a clearly prove the important contribution of bulk current to flicker noise, since increasing KCl concentration from 10 mM to 1 M at a constant *p*H=5 has led to a continuous increase in the 1/*f* noise.

A smaller pore of 40 nm in diameter was used in Figure 4b to enhance the surface effect. The noise was measured at a constant current bias of 100 nA and the *p*H value was successively increased from 2.5 to 11, but with an invariant KCl concentration at 100 mM. The results in Figure 4b undoubtedly show variations of flicker noise by changing *p*H value, but not in a monotonous manner. The noise PSD level first increases with increasing *p*H to around 5. Further increase in *p*H value leads to decrease in noise PSD. The maximum noise PSD level appears *p*H~5, which is close to the point of zero charge of SiN_x.[46] Since the bulk current is kept constant and so is its noise component, the observed *p*H related variations of noise PSD can only be attributed to the change in surface charge density, thereby confirming the contribution of surface current to flicker noise. As a final proof, the flicker noise of smaller-diameter pores shows a stronger *p*H dependence when the noise PSD is compared for nanopores of different sizes (see Supporting Information Figure S8), since larger effects of surface current are expected for smaller-diameter pores.

D. Noise model and modeling results

The clear trends observed in Figures 2 and 3 constitute the basis for the development of a comprehensive and generalized model of LF noise in SSNs in this B-section. Apart from the white thermal noise from the nanopore resistance expressed in eq. (2), the 1/*f* noise includes two contributions: flicker noise from the nanopore and the 1/*f*-shape noise from the electrodes. The flicker noise comprises components from the EDL region around the SSN and from the bulk in the nanopore beyond the EDL. Hence, the complete model of LF noise should read:

$$\begin{aligned} S_I(f) &= S_{IS} + S_{IB} + S_{IE} + S_{IT} + S_{ID} \\ &= \frac{\alpha_H I_S^2}{N_{C,S} f^\beta} + \frac{\alpha_H I_B^2}{N_{C,B} f^\beta} + \frac{a_e}{f^\beta} + \frac{4kT}{R} + 8\pi kTdC_{chip} f \end{aligned} \quad (4)$$

where, S_{IS}, S_{IB}, S_{IE}, S_{IT}, and S_{ID} represent the current noise PSD components for surface flicker noise, bulk flicker noise, electrode noise, white thermal noise, and dielectric noise, respectively; I_S and I_B are the surface and bulk current, respectively; $N_{C,S}$ and $N_{C,B}$ are the total number of charge carriers inside the EDL (surface) and the bulk; a_e is the current noise parameter for the electrodes; d is the dielectric loss factor of the membrane capacitance; C_{chip} is the capacitance of the membrane on which the nanopore is drilled. Derivation of eq. (4) is found in Appendix. According to the widely used conductance model for nanopores,[36,37] the nanopore resistance can be calculated based on the nanopore size and KCl concentration. Thus, I_S and I_B can be derived separately at a specified voltage bias. Except for α_H, β, and a_e that can be obtained through fitting the model to the measured noise PSD curves, all other parameters are determined with their respective values given in Table S1 (Supporting Information). A high fidelity of model fitting to the experimental noise PSD results can be concluded from Figure 5a-c for the 65 nm nanopore with 10 mM, 100 mM and 1 M KCl, respectively. The fitting yields a_H and a_e for each data group, while β is tuned from 1 to 1.7 in order to give the most optimized match at all current biases but for a given KCl concentration.

Hence, our noise model captures the main features of the SSN noise and can be used for analysis of the general noise behavior of SSNs. The extracted values of α_H and a_e from 18 groups of data are shown in Figure 5d-e, respectively. The extracted α_H data points have an average value of 1.9×10^{-4}, which agrees well with the Hooge parameter reported by others.[19,30,47] The noise parameter for the electrodes, a_e, increases almost linearly with KCl concentration and this behavior validates our earlier conclusion that higher KCl concentrations give rise to lower solution resistances and thus higher current noise levels from the electrodes.

The model is also used to illustrate the contribution of surface current to the total flicker noise as a function of KCl concentration and nanopore diameter. This contribution in Figure 6 is measured in percentages of the total flicker noise including both surface and bulk components. Note that the membrane thickness has no influence on the flicker noise as the access region[17] close to the nanopore is not considered in the model. As expected, the surface flicker noise predominates (i.e. >50%) at low KCl concentrations and for small-diameter pores, since under such conditions the EDL occupies a considerable fraction of the pore opening and the surface plays a predominant role. The dominance of the two flicker noise components in the LF noise is clearly shown in Supporting Figure S9. The contribution from either the solution resistance (thermal) or the Ag/AgCl electrodes is almost negligible.

The model is further used to predict the noise RMS for pores of very small dimensions (diameters 2 and 5 nm and membrane thicknesses 1 and 2 nm) where the surface flicker noise prevails. The squared noise RMS values (for them to be added) in the LF range (0.1 Hz-1 kHz) are found to vary much more strongly with KCl concentration than with current bias, as shown in Supporting Figure S10. The nanopores are characterized by higher noise in more dilute solution under larger current bias. The results point to severe challenges with rising

noise level when using small-diameter pores in thin membranes to boost signal and improve base resolution in DNA sequencing.[17]

E. Strategies for signal enhancement and noise control

It is commonly acknowledged that the pore dimensions should become comparable with the size of biomolecules to be detected in order to enhance signal in nanopore sensing including DNA sequencing.[11] However, shrinking the pore diameter directly leads to the predominance of the surface current contribution and a decrease in number of carriers thereby increase in fluctuation of ionic current. This signal-noise dilemma may find remedies by examining the root causes of noise and the relationship between noise and operational conditions. Since the flicker noise from the nanopore surface is predominant for small-diameter pores, it is possible to suppress it by increasing the surface charge density through, e.g. tuning the *p*H value of the salt solution as shown in Figure 4b and Figure S8, coating the pores with functional layers, etc. Understanding the noise behavior of solid-state nanopores is, therefore, of significant implications in design and operation of nanopore devices to attain large signal and low noise in applications including DNA sequencing, protein analysis, and biochemical detection in general.

Conclusions

Based on the noise PSD measured on SiN_X nanopores of a wide range of diameters and with salt solutions of different KCl concentrations and *p*H values, we have identified several major sources of LF noise: fluctuation of ionic current in the nanopores (i.e. the flicker noise) and fluctuation of charge carriers at the electrode-solution interface (i.e. the 1/*f*-shape noise from

the Ag/AgCl electrodes). The noise from the electrodes behaves as a voltage source and induces current fluctuation on the solution resistance of the nanopore. The flicker noise arises from fluctuations in both surface and bulk current. The former is determined by the surface charge density that can be tuned by varying *p*H value, while the latter is influenced by the salt concentration. The improved understanding has led to the establishment of a generalized model encompassing most noise mechanisms especially in the LF range. The model results agree well with the experimental data for a wide range of nanopore diameters with in a large span of KCl concentrations. The surface component of the flicker noise becomes more dominant in smaller nanopores with lower salt concentrations. The relative importance of surface versus bulk flicker noise is largely proportional to their conductance ratio. Knowledge gained in this study can be employed for guiding design and operation of the nanopore sensor devices.

Methods

Fabrication of SiN_x nanopores. Our nanopore fabrication started from a 300 μm thick silicon (100) wafer with double-side polished surfaces. A layer of 50 nm thick SiO_2 was first grown on the substrate wafer by dry oxidation, followed by the deposition of a 20 nm thick low-stress SiN_x film in a low-pressure chemical vapor deposition (LPCVD) reactor. To fabricate the SiN_x membrane structure, a 425 μm × 425 μm square window was opened on the rear side of the wafer by a combination of photolithography and reactive ion etching (RIE) to remove the SiN_x and SiO_2 in the window, followed by wet etching of the bulk silicon substrate in KOH (30 wt%, 80 ^{o}C, 5 h) and then the front SiO_2 in buffered HF (40 s). Those process steps left the remaining front 20 nm thick SiN_x film as a free-standing membrane. Since the wet silicon etch by KOH is strongly surface orientation dependent, e.g. etch of the

(111) surface being much slower than that of the (100) surface, the window became 20 μm × 20 μm right at the SiN_x membrane. When the SiN_x membrane was ready, the nanopore was drilled either with gallium ions on a focus ion beam system (FIB, Strata DB235, FEI Company) with an operation voltage of 30 kV or with helium ions on a Helium Ion Microscope (Zeiss Orion). Different diameters were obtained by changing the exposure time and/or beam current.

Electrical measurement setup. The nanopore chip was sandwiched by two homemade lids each containing its own inlet and outlet for salt solution injection (shown in Figure S1a). An Ag/AgCl electrode (2 mm in diameter, Warner Instruments, LLC.) was mounted in the middle of each lid with a silicon rubber O-ring (8 mm in diameter and 1 mm in thickness) set between the chip and the lid in order to prevent solution leakage. The sealed containers on both sides of the nanopore chip have a volume around 50 μL. The ionic current in the nanopore was picked up and amplified using Axon Axopatch 200B (Molecular Device LLC.) with an input capacitance around 70 pF, digitalized by Axon Digidata 1550A (Molecular Device LLC.), and recorded by the software Axon pCLAMP 10 (Molecular Device LLC.). The RMS value of noise was simultaneously monitored using digital multimeter (34411A, Keysight Technology).

ASSOCIATED CONTENT

Supporting Information. The Supporting Information is available free of charge on the ACS Publications website at ....

The following files are available free of charge.

Analysis of the noise from the Ag/AgCl electrodes; the noise PSD of a 7.2 nm nanopore; the dependence of surface charge density on KCl concentration; the *p*H dependent noise in

nanopores of different sizes; the noise level predicted by our model; the parameters used in the model for fitting. (PDF)

AUTHOR INFORMATION

Corresponding Author

*Zhen Zhang. * To whom correspondence should be addressed: zhen.zhang@angstrom.uu.se

Author Contributions

‡These authors contributed equally.

Notes

The authors declare no competing financial interest

ACKNOWLEDGMENT

The authors would like to thank Dr. Paul Solomon and Da Zhang for fruitful discussions. This work was supported by the Swedish Research Council (621-2014-6300), Stiftelsen Olle Engkvist Byggmästare (2016/39), the Wallenberg Academy Fellow Program, the Swedish Strategic Research Foundation (5th Ingvar Carlsson Award and 6th Future Research Leader programs), and the Finnish Centre of Excellence on Nuclear and Accelerator Based Physics by the Academy of Finland (251353). CW was a scholarship recipient of the China Scholarship Council.

REFERENCES

[1] Deamer, D.; Akeson, M.; Branton, D. Three Decades of Nanopore Sequencing. *Nat. Biothchnol.* **2016**, *34*, 518-524.

[2] Venkatesan, B. M.; Bashir, R. Nanopore Sensors for Nucleic Acid Analysis. *Nat. Nanotechnol.* **2011**, *6*, 615-624.

[3] Tagliazucchi, M.; Szleifer, I. Transport Mechanisms in Nanopores and Nanochannels: Can We Mimic Nature? *Mater. Today* **2015**, *18*, 131-142.

[4] Dekker, C. Solid-state Nanopores. *Nat. Nanotechnol.* **2007**, *2*, 209-215.

[5] Healy, K.; Schiedt, B.; Morrison, A. P. Solid-State Nanopore Technologies for Nanopore-Based DNA Analysis. *Nanomedicine* **2007**, *2*, 875-897.

[6] Ayub, M.; Hardwick, S. W.; Luisi, B. F.; Bayley, H. Nanopore-Based Identification of Individual Nucleotides for Direct RNA Sequencing. *Nano Lett.* **2013**, *13*, 144-6150.

[7] Wei, R.; Gatterdam, V.; Wieneke, R.; Tampe, R.; Rant, U. Stochastic Sensing of Proteins with Receptor-Modified Solid-State Nanopores. *Nat. Nanotechnol.* **2012**, *2*, 257-263.

[8] Howorka, S.; Siwy, Z. Nanopore Analytics: Sensing of Single Mmolecules. *Chem. Soc. Rev.* **2009**, *38*, 2360–2384.

[9] Wu, H.-C.; Astier, Y.; Maglia, G.; Mikhailova, E.; Bayley, H. Protein Nanopores with Covalently Attached Molecular Adapters. *J. Am. Chem. Soc.* **2007**, *129*, 16142-16148.

[10] Tsutsui, M.; Hongo, S.; He, Y.; Taniguchi, M.; Gemma, N.; Kawai. T.; Single-Nanoparticle Detection Using a Low-Aspect-Ratio Pore. *ACS Nano* **2012**, *4*, 3499-3505.

[11] Muthukumar, M.; Plesa, C.; Dekker, C. Single-Molecule Sensing with Nanopores. *Phys. Today* **2015**, *68*, 40-46.

[12] Kasianowicz, J. J.; Brandin, E.; Branton, D.; Deamer; D. W. Characterization of Individual Polynucleotide Molecules Using a Membrane Channel. *Proc. Natl. Acad. Sci. USA* **1996**, *93*, 13770–13773.

[13] Akeson, M.; Branton, D.; Kasianowicz, J. J.; Brandin, E.; Deamer, D. W. Microsecond Time-Scale Discrimination Among Polycytidylic Acid, Polyadenylic Acid, and Polyuridylic Acid as Homopolymers or as Segments Within Single RNA Molecules. *Biophys. J.* **1999**, *77*, 3227–3233.

[14] Jain, M.; Fiddes, I. T.; Miga, K. H.; Olsen, H. E.; Paten, B.; Akeson, M. Improved Data Analysis for the MinION Nanopore Sequencer. *Nat. Methods* **2015**, *12*, 351-356.

[15] Magierowski, S.; Huang, Y.; Wang, C.; Ghafar-Zadeh, E. Nanopore-CMOS Interfaces for DNA Sequencing. *Biosensors* **2016**, *6*, 42.

[16] Tabard-Cossa, V.; Trivedi, D.; Wiggin, M.; Jetha, N. N.; Marziali, A. Noise Analysis and Reduction in Solid-State Nanopores. *Nanotechnology* **2007**, *18*, 305505.

[17] Wen, C.; Zeng, S.; Zhang, Z.; Hjort, K.; Scheicher, R.; Zhang, S.-L. On Nanopore DNA Sequencing by Signal and Noise Analysis of Ionic Current. *Nanotechnology* **2016**, *27*, 215502.

[18] Heerema, S. J.; Schneider, G. F.; Rozemuller, M.; Vicarelli, L. Zandbergen, H. W.; Dekker, C. 1/f Noise in Graphene Nanopores. *Nanotechnology* **2015**, *26*, 074001.

[19] Smeets, R. M. M.; Dekker, N. H.; Dekker, C. Low-frequency Noise in Solid-State Nanopores. *Nanotechnology* **2009**, *20*, 095501.

[20] Powell, M. R.; Vlassiouk, I.; Martens, C.; Siwy, Z. S. Nonequilibrium 1/f Noise in Rectifying Nanopores. *Phys. Rev. Lett.* **2009**, *103*, 248104.

[21] Tasserit, C.; Koutsioubas, A.; Lairez, D.; Zalczer, G.; Clochard, M.-C. Pink Noise of Ionic Conductance through Single Artificial Nanopores Revisited. *Phys. Rev. Lett.* **2010**, 105, 260602.

[22] Powell, M. R.; Martens, C.; Siwy, Z. S. Asymmetric Properties of Ion Current 1/f Noise in Conically Shaped Nanopores. *Chem. Phys.* **2010**, *375*, 529–535.

[23] Powel, M. R.; Sa, N.; Davenport, M.; Healy, K.; Vlassiouk, I.; Létant, S. E.; Baker, L. A.; Siwy, Z. S. Noise Properties of Rectifying Nanopores. *J. Phys. Chem. C* **2011**, *115*, 8775–8783.

[24] Balan, A.; Machielse, B.; Niedzwiecki, Da.; Lin, J.; Ong, P.; Engelke, R.; Shepard, K. L.; Drndić, M. Improving Signal-to-Noise Performance for DNA Translocation in Solid-State Nanopores at MHz Bandwidths. *Nano Lett.* **2014**, *14*, 7215-7220.

[25] Levis, R. A.; Rae, J. L. The Use of Quartz Patch Pipettes for Low Noise Single Channel Recording. *Biophys. J.* **1993**, *65*, 1666-1677.

[26] Smeets, R. M. M.; Keyser, U. F.; Wu, M.Y.; Dekker, N. H.; Dekker, C. Nanobubbles in Solid-State Nanopores. *Phys. Rev. Lett.* **2006**, *97*, 088101.

[27] Uram, J. D.; Ke, K.; Mayer, M. Noise and Bandwidth of Current Recordings from Submicrometer Pores and Nanopores. *ACS Nano* **2008**, *2*, 857-872.

[28] Lee, M.-H.; Lee, J.-H.; Kim, H.-M.; Kim, Y.-R.; Jeon, T.-J.; Pak, Y. E.; Kim, K.-B. Leakage Current in a Si-Based Nanopore Structure and Its Influence on Noise Characteristics. *Mocrofluid. Nanofluid.* **2014**, *16*, 123-130.

[29] Dimitrov,V.; Mirsaidov, U.; Wang, D.; Sorsch, T.; Mansfield, W.; Miner, J.; Klemens, F.; Cirelli, R.; Yemenicioglu, S.; Timp, G. Nanopores in Solid-State Membranes Engineered for Single Molecule Detection. *Nanotechnology* **2010**, *21*, 065502.

[30] Kumar, A.; Park, K.-B.; Kim, H.-M.; Kim, K.-B. Noise and Its Reduction in Graphene Based Nanopore Devices. *Nanotechnology* **2013**, *24*, 495503.

[31] Chen, P.; Mitsui, T.; Farmer, D. B.; Golovchenko, J.; Gordon, R. G.; Branton D. Atomic Layer Deposition to Fine-Tune the Surface Properties and Diameters of Fabricated Nanopores. *Nano Lett.* **2004**, *4*, 1333-1337.

[32] Rosenstein, J. K.; Wanunu, M.; Merchant, C. A.; Drndic, M.; Shepard, K. L. Integrated Nanopore Sensing Platform with Sub-Microsecond Temporal Resolution, *Nat. Methods* **2012**, *9*, 487-492.

[33] Shekar, S.; Niedzwiecki, D. J.; Chien, C.-C.; Ong, P.; Fleischer, D. A.; Lin, J.; Rosenstein, J. K.; Drndić, M.; Shepard, K. L. Measurement of DNA Translocation Dynamics in a Solid-State Nanopore at 100 ns Temporal Resolution. *Nano Lett.* **2016**, *16*, 4483−4489.

[34] Goldstein, B.; Kim, D.; Xu, J.; Vanderlick, T. K.; Culurciello, E. CMOS Low Current Measurement System for Biomedical Applications. *IEEE Trans. Biomed. Circuits Syst.* **2012**, *6*, 111-119.

[35] Arjmandi-Tash, H.; Belyaeva, L. A.; Schneider, G. F. Single Molecule Detection with Graphene and Other Two-Dimensioxnal Materials: Nanopores and Beyond. *Chem. Soc. Rev.* **2016**, *45*, 476–493.

[36] Ralph, M. M.; Smeets, U. F.; Keyser, D. K.; Wu, M.-Y.; Dekker, N. H.; Dekker, C. Salt Dependence of Ion Transport and DNA Translocation through Solid-State Nanopores. *Nano Lett.* **2006**, *6*, 89-95.

[37] Lee, C.; Joly, L.; Siria, A.; Biance, A.-L.; Fulcrand, R.; Bocquet, L.; Large Apparent Electric Size of Solid-State Nanopores Due to Spatially Extended Surface Conduction. *Nano Lett.* **2012**, *12*, 4037-4044.

[38] Siwy, Z.; Fuliński. A.; Origin of 1=f$^{\alpha}$ Noise in Membrane Channel Currents. *Phys. Rev. Lett.* **2002**, *89*, 158101.

[39] Levis, R. A.; Rae, J. L. The Use of Quartz Patch Pipettes for Low Noise Single Channel Recording. *Biophys. J.* **1993,** *65*, 1666-1677.

[40] Balan, A.; Machielse, B.; Niedzwiecki, D.; Lin, J.; Ong, P.; Engelke, R.; Shepard, K. L.; Drndić, M. Improving Signal-to-Noise Performance for DNA Translocation in Solid-State Nanopores at MHz Bandwidths. *Nano Lett.* **2014**, *14*, 7215−7220.

[41] Hung, K. K.; Ko, P. K.; Hu, C.; Cheng, Y. C. A Unified Model for the Flicker Noise in Metal-Oxide-Semiconductor Field-Effect Transistors. *IEEE Trans. Electron Devices*, **1990**, *37*, 654-665.

[42] Zhang, D.; Must, I.; Netzer, N. L.; Xu, X.; Solomon, P.; Zhang, S.-L.; Zhang. Z.; Direct Assessment of Solid–Liquid Interface Noise in Ion Sensing Using a Differential Method. *App. Phys. Lett.* **2016**, *108*, 151603.

[43] Fiori, N. D.; Squires, A.; Bar, D.; Gilboa, T.; Moustakas, T. D.; Meller, A. Optoelectronic Control of Surface Charge and Translocation Dynamics in Solid-State Nanopores. *Nat. nanotechnol.* **2013**, *8*, 946-951.

[44] He, Y.; Tsutsui, M.; Fan, C.; Taniguchi, M.; Kawai, T. Gate Manipulation of DNA Capture into Nanopores. *ACS Nano* **2011**, *5*, 8391-8397.

[45] Van Hal, R. E. G.; Eijkel, J. C. T.; Bergveld, P. A General Model to Describe the Electrostatic Potential at Electrolyte Oxide Interfaces. *Adv. Colloid Interface Sci.* **1996**, *69*, 31-62.

[46] Kosmulski, M. The pH-Dependent Surface Charging and the Points of Zero Charge. *J. Colloid Interface Sci.* **2002**, 253, 77–87.

[47] Smeets, R. M. M.; Keyser, U. F.; Dekker, N. H.; Dekker, C. Noise in Solid-State Nanopores. *Proc. Natl. Acad. Sci. USA* **2008**, *105*, 417-421.

Appendix – The generalized noise model

The low-frequency noise from a solid-state nanopore is composed of four components: the flicker noise from the pore S_{IF}, the 1/*f*-shape noise from the Ag/AgCl electrodes S_{IE}, the white thermal noise S_{IT}, and the dielectric noise S_{ID}:

$$S_I(f) = S_{IF} + S_{IE} + S_{IT} + S_{ID} \quad \text{(A1)}$$

Since the flicker noise in the pore is contributed by both surface and bulk currents, the following is valid:

$$S_{IF} = S_{IS} + S_{IB} \quad \text{(A2)}$$

According to Hooge's theory on flicker noise:

$$S_{IS} = \frac{\alpha_H I_S^2}{N_{C,S} f^\beta},\ S_{IB} = \frac{\alpha_H I_B^2}{N_{C,B} f^\beta} \quad \text{(A3a,b)}$$

where, *f* is frequency; β is a constant ranging from 0 to 2; α_H is a constant named Hooge parameter; $N_{C,S}$ and $N_{C,B}$ are the total number of carriers in the surface and bulk region, respectively; I_S and I_B are the current in the surface and bulk region, respectively. For a given nanopore in a solution of a specified KCl concentration, the solution resistance, *R*, is the sum of pore resistance and access resistance:[36]

$$R = \frac{H}{\pi D}[ecN_A(\mu_+ + \mu_-)\frac{D}{4} + \sigma\mu_+]^{-1} + [ecN_A(\mu_+ + \mu_-)D]^{-1} \quad \text{(A4)}$$

where, *H* is the membrane (nanopore) thickness, *D* is the nanopore diameter, *e* is element charge, *c* is salt concentration, N_A is the Avogadro constant, μ+ and μ- are the mobility of cation and anion, respectively, and σ is the surface charge density. At voltage bias *U*, the current in the surface and bulk regions can be expressed as:

$$I_S = U\sigma\mu_K \frac{\pi D}{H} \quad \text{(A5a)}$$

$$I_B = Uec(\mu_K + \mu_{Cl})\frac{\pi D^2}{4H} \quad \text{(A5b)}$$

The total carrier numbers in the surface and bulk regions are:

$$N_{C,S} = \sigma \pi DH \tag{A6a}$$

$$N_{C,B} = \frac{\pi}{2} D^2 HcN_A \tag{A6b}$$

For the 1/*f*-shape noise from the electrodes, it can be expressed as:

$$S_{IE} = \frac{a_e}{f^\beta} \tag{A7}$$

where, a_e is a coefficient representing the noise intensity from the electrodes. Finally, the white thermal noise and dielectric noise are, respectively:

$$S_{IT} = \frac{4kT}{R} \tag{A8}$$

$$S_{ID} = 8\pi kTdC_{chip} f \tag{A9}$$

where, k is Boltzmann constant; T is temperature in K; R is the solution resistance; d is the dielectric loss factor of the membrane capacitance; and C_{chip} is the membrane capacitance. Thus, the total current noise of the solid-state nanopore becomes:

$$S_I(f) = \frac{\alpha_H I_S^2}{N_{C,S} f^\beta} + \frac{\alpha_H I_B^2}{N_{C,B} f^\beta} + \frac{a_e}{f^\beta} + \frac{4kT}{R} + 8\pi kTdC_{chip} f \tag{A10}$$

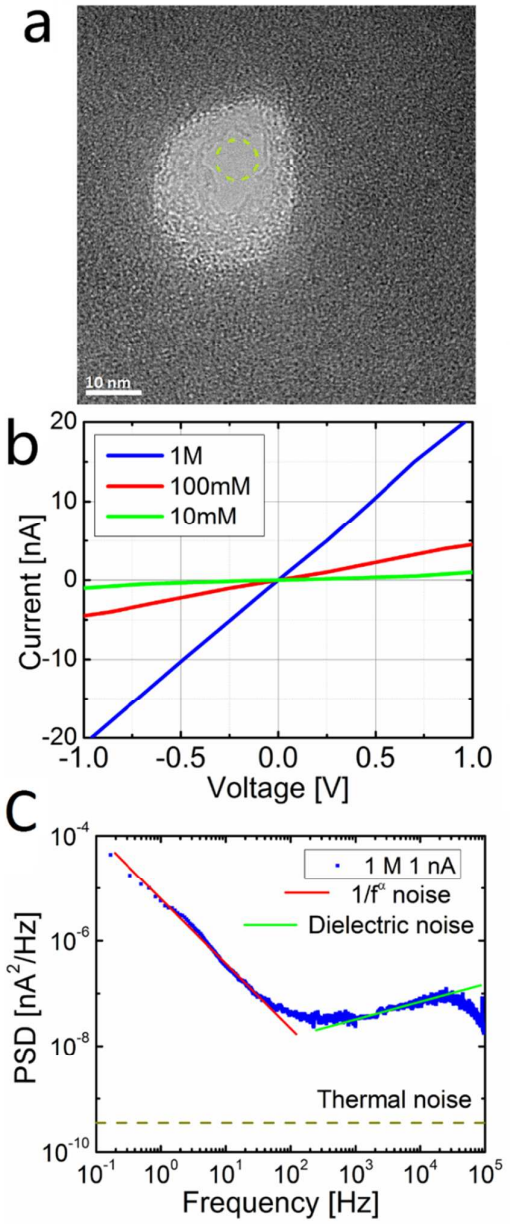

Figure 1. General SiN_x nanopore characteristics of a 7.2 nm pore. (a) TEM image of the nanopore with the green dash line to indicate how a 7.2 nm pore would fit in. Scale bar: 10 nm. (b) Voltage-current characteristics at three different KCl concentrations. (c) Typical noise PSD in 1 M KCl solution under 1 nA current bias.

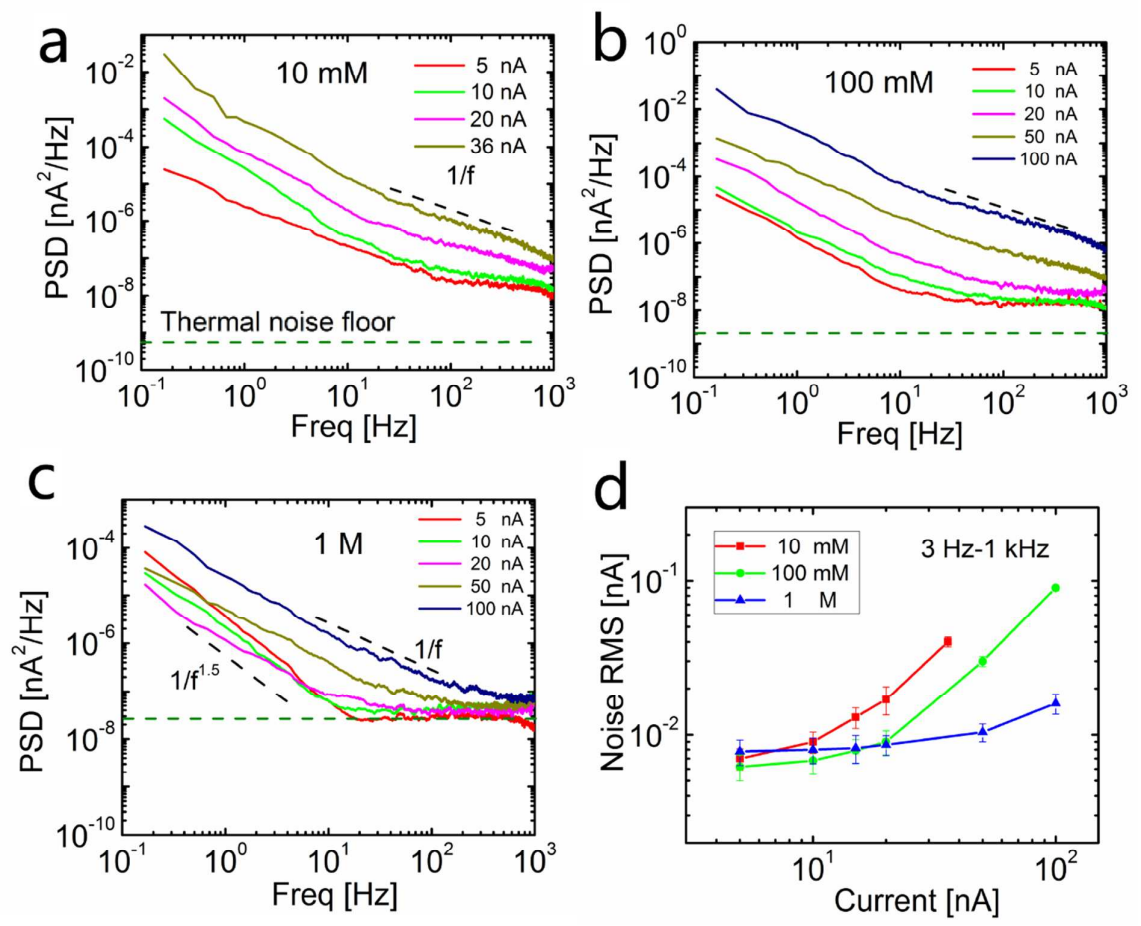

Figure 2. Noise PSD of a 65 nm SiN_x nanopore in salt solutions of different KCl concentrations. (a-c) Noise PSD under different current biases at 5 to 100 nA in 10 mM, 100 mM, and 1 M KCl solution, respectively. (d) Variation of noise RMS with current bias for the three different KCl concentrations.

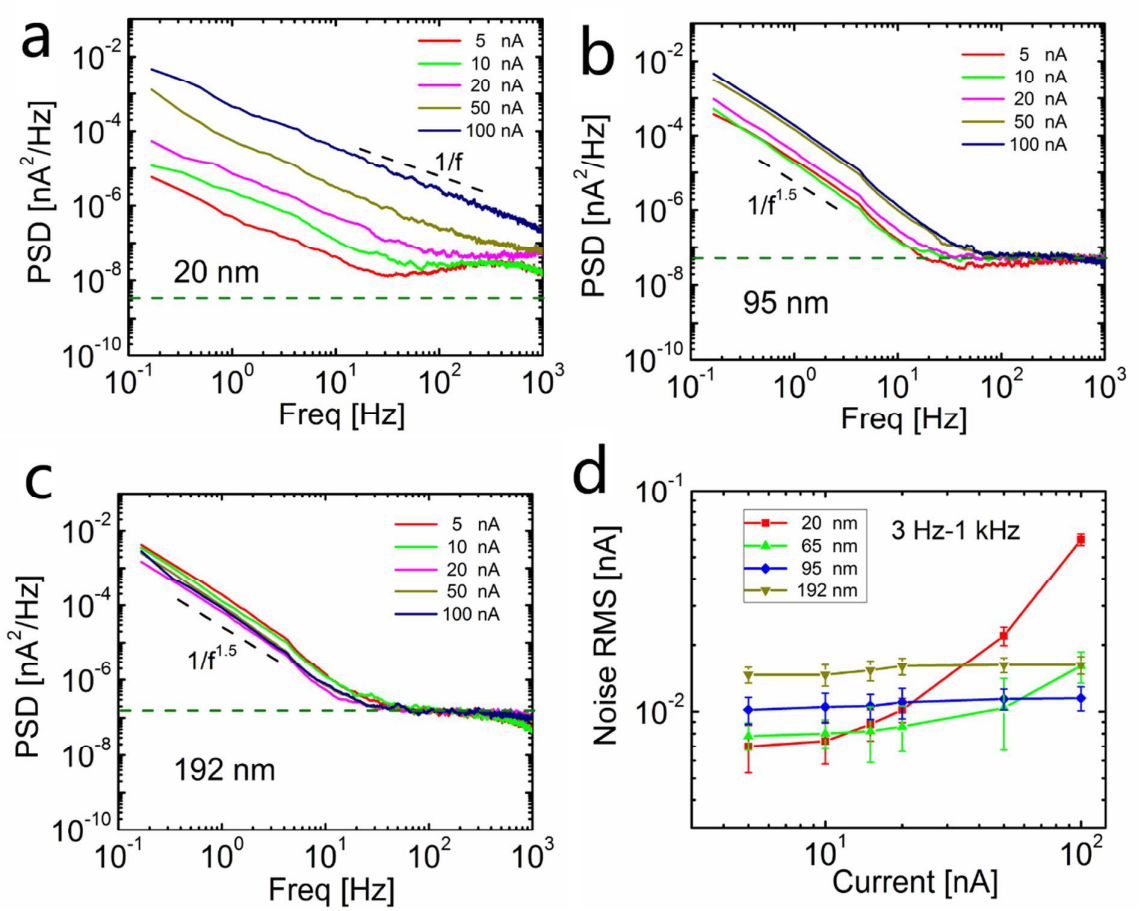

Figure 3. Noise PSD of SiN_x nanopores of different sizes in 1 M KCl solution. (a-c) Noise PSD of the nanopores of 20, 95, and 192 nm in diameter, respectively. (d) Variation of noise RMS with current bias for the four nanopores, with the data for the 65 nm nanopore from Figure 2c.

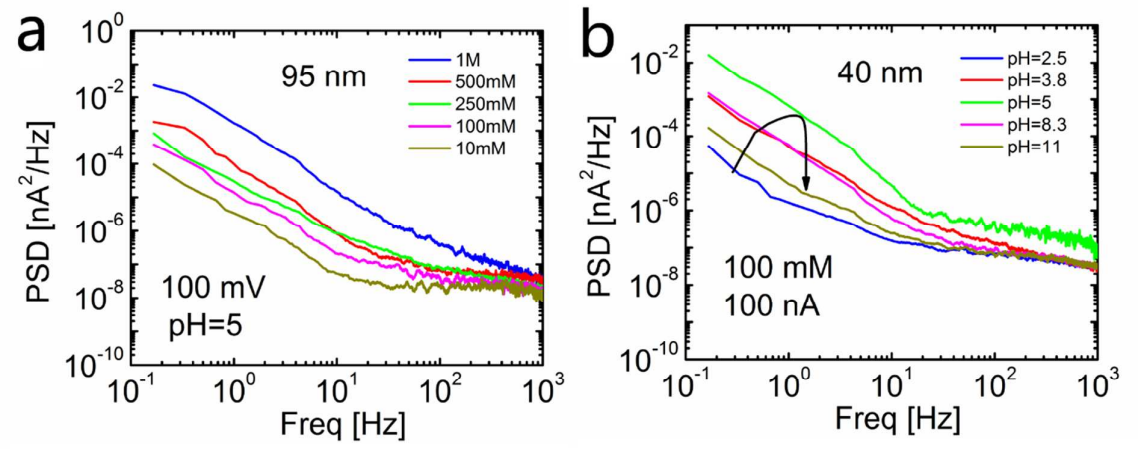

Figure 4. Dependence of noise PSD on salt concentration and *p*H value. (a) Noise PSD of the 95 nm nanopore in salt solutions of different KCl concentrations under a constant voltage bias of 100 mV and with *p*H=5. (b) Noise PSD of a 40 nm nanopore in salt solutions of 100 mM KCl but different *p*H values, under a constant current bias of 100 nA, with the curled arrow helping show how the noise level first increases and then decreases with increasing *p*H value.

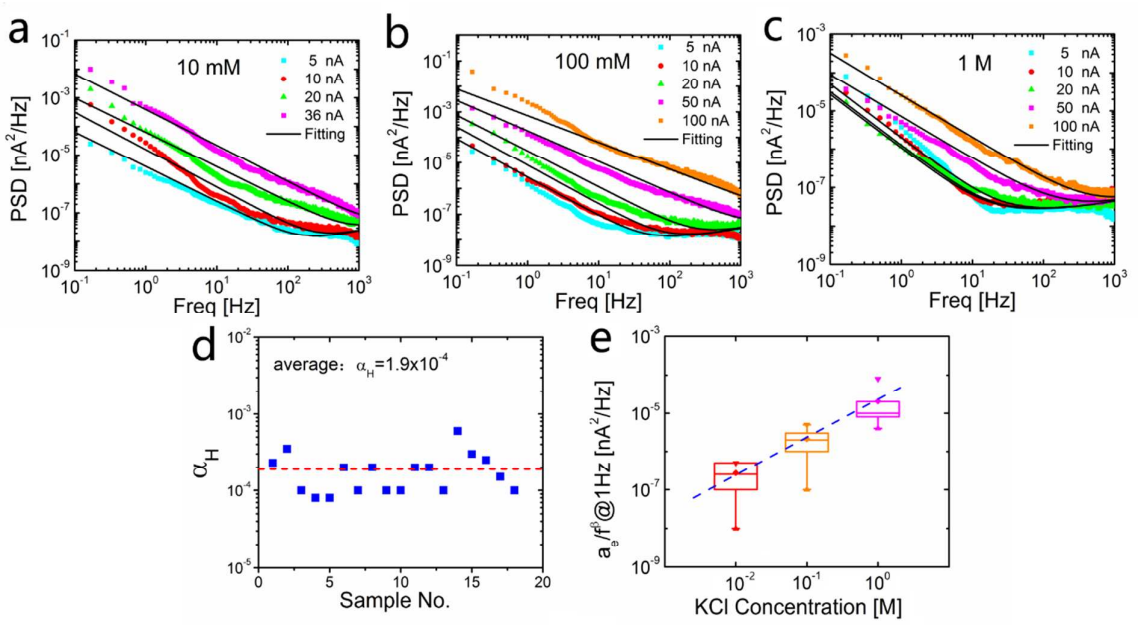

Figure 5. Model application. (a-c) Model fitting to the noise PSD of the 65 nm nanopore under different current biases in salt solutions of 10 mM, 100 mM, and 1 M KCl concentrations, respectively. (d) Hooge parameter extracted from 18 groups of noise PSD data, with the horizontal red dash line representing the average. (e) Variation of extracted current noise parameter from the electrodes, a_e, with KCl concentration.

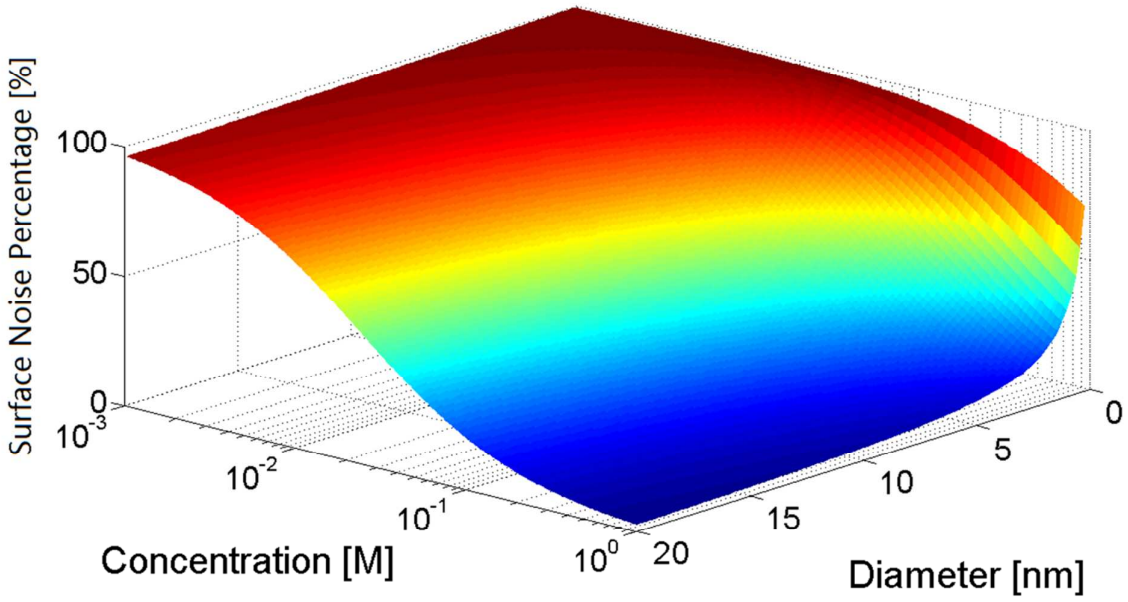

Figure 6. Contribution of the surface noise to the total flicker noise measured in percentages versus nanopore diameter and KCl concentration.

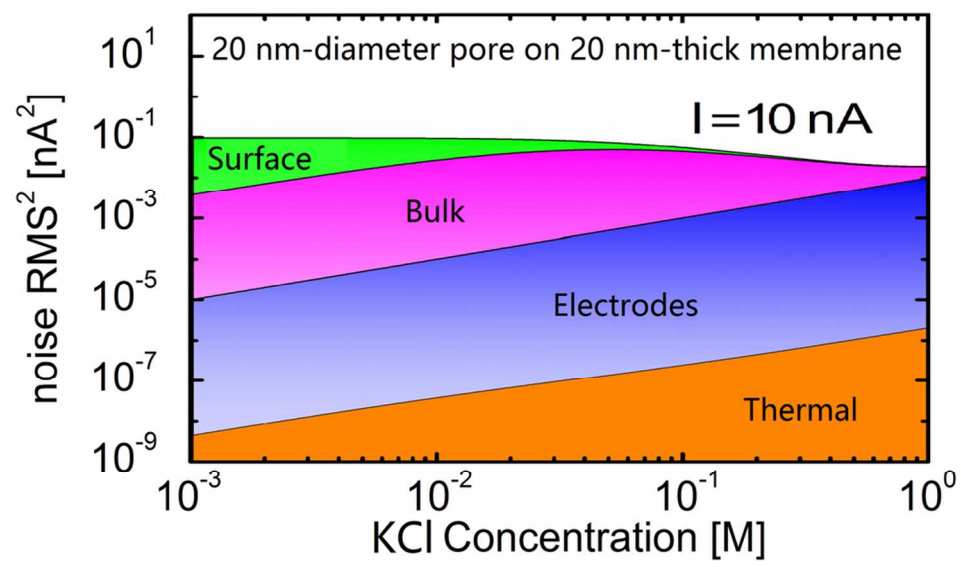

Table of contents graphic

47x26mm (600 x 600 DPI)